Physics of Fluids ARTICLE scitation.org/journal/phf

# Solute dispersion in transient Casson fluid flow through stenotic tube with exchange between phases

Cite as: Phys. Fluids **33**, 061907 (2021); doi: 10.1063/5.0052770
Submitted: 1 April 2021 · Accepted: 27 May 2021 ·
Published Online: 21 June 2021



Prosanjit Das,[1] Sarifuddin,[2] Jyotirmoy Rana,[3] and Prashanta Kumar Mandal[1,a)]

## AFFILIATIONS

[1]Department of Mathematics, Visva-Bharati University, Santiniketan, West Bengal 731235, India
[2]Department of Mathematics, Berhampore College, Berhampore, Murshidabad, West Bengal 742101, India
[3]School of Naval Architecture, Ocean and Civil Engineering, Shanghai Jiao Tong University, Shanghai 200240, China

[a)]**Author to whom correspondence should be addressed:** prashantakumar.mandal@visva-bharati.ac.in

## ABSTRACT

A mathematical study on solute dispersion has been carried out in a stenotic tube having an absorptive wall—a study relevant to arterial pharmacokinetics. The rheology of blood is represented by Casson model and the solute is introduced at a point that is uniformly distributed over the cross section. The two-dimensional fluid flow is considered in this study. The governing equations of motion for the flow of Casson fluid, for the transport of solute in the lumen as well as in the tissue along with appropriate initial and boundary conditions, are numerically solved by leveraging the Marker and Cell method and the immersed boundary method in staggered grids formulation. Following the introduction of solute, we provide a comprehensive investigation of the influence of the wall absorption parameter ($\kappa$), yield stress ($\tau_y$), and the severity of the stenosis ($\xi$) on the three transport coefficients, namely, the fraction of solute remaining in the fluid phase, the apparent convection velocity, and the dispersion coefficient. Simulated results predict the diminishing magnitudes of the transport coefficients with the increase in the values of yield stress and absorption parameter. Moreover, the transport coefficients and the axial mean concentration get significantly perturbed by the severity of the stenosis. Obtained results presented graphically concur with existing steady-state results in the literature. The present study would certainly be of some use in the case of targeted drug delivery and in treatment related to microvascular disease.



## NOMENCLATURE

| | |
|---|---|
| $C_f, C_w$ | fluid phase and wall phase concentration, respectively |
| $D_f, D_w$ | fluid phase and wall phase diffusion coefficient, respectively |
| $H$ | Heaviside function |
| $J_2$ | rate of strain tensor invariant |
| $J_2^*$ | second invariant of the stress tensor |
| $Pe_f$ | Peclet number |
| $p$ | pressure |
| $Re$ | Reynolds number |
| $(r, \theta, z)$ | cylindrical coordinate |
| $r_c$ | radius of the plug region |
| $r_0$ | dimensional upstream radius |
| $t$ | time |
| $U_0$ | centerline velocity in a Poiseuille flow |
| $u_z, u_r$ | axial and radial velocity, respectively |
| $z_0$ | half-length of the stenosis |

### Greek

| | |
|---|---|
| $\beta$ | ratio of wall phase concentration to fluid phase concentration at equilibrium |
| $\delta$ | Dirac delta function |
| $\eta$ | viscosity coefficient of Casson fluid |
| $\kappa$ | absorption parameter |
| $\lambda$ | ratio of the diffusion coefficients |
| $\mu(J_2)$ | apparent viscosity |
| $\xi$ | maximum height of the stenosis |
| $\rho$ | fluid density |
| $\tau_{ij}$ | shear stress |
| $\tau_y$ | yield stress of Casson fluid |

$\phi_{ij}$ rate of strain tensor
$\omega$ relaxation parameter for S.O.R scheme

## I. INTRODUCTION

The transportation of solute dispersion process has been widely studied due to its extensive application in the field of chemical engineering, physiological fluid dynamics, environmental sciences, and pharmacology (cf. Phillips *et al.*,[1] Or and Ghezzehei,[2] Singhal and Gupta,[3] Dejam and Hassanzadeh,[4] Gat *et al.*,[5] and Das *et al.*[6]). Studies on the dispersion of solute, such as drug, toxin, or nutrient, in blood flow through a narrow artery having, a linear or constricted wall received much attention owing to its significant contribution in understanding the issues in biomedical engineering and cardiovascular mechanics. Constriction in an artery occurs because of the accumulation of low-density lipoprotein (LDL) and other macromolecules along the inner lining of the arterial wall. The formation of such lesion or plaque started blocking the artery and reducing the normal blood flow, medically termed as "atherosclerosis."[7] It is important for clinicians to analyze the rate of dispersion of an injected drug associated with intravenous drug delivery into an affected artery because of its therapeutic nature and also to measure the amount of drug in the system for better efficacy as well as the effectiveness of the delivery.

Dispersion through the smaller tube considering Newtonian or non-Newtonian fluid flow has been investigated by some assiduous researchers. In a pioneering work, Taylor[8] introduced the concept of dispersion in fluid flow and, later, Aris[9] extended the analysis of Taylor's dispersion by suppressing some constraints. In the presence of pulsatile flow, Aris[10] determined the effective dispersion coefficient of solute by using the method of moments. A numerical study was performed by Ananthakrishnan[11] to discuss the effect of Peclet number on the dispersion process and validated the Taylor–Aris results for large timescale. On account of all time analysis of dispersion, Gill and Sankarasubramanian[12] proposed a generalized dispersion model. Further, Gill and Sankarasubramanian[13] investigated the dispersion phenomena using the generalized dispersion model for Casson fluid flow through a tube having an absorptive boundary, under consideration of exchange coefficient, convective coefficient, and dispersion coefficient.

Mukherjee and Mazumder[14] investigated the effect of pulsatile Newtonian flow past a circular tube and parallel plates on the dispersion of the cloud of contaminant using the method of moments. Mazumder and Das[15] analyzed the axial dispersion of a passive contaminant in a time-dependent laminar flow in the presence of a reactive wall. Phillips *et al.*[1] considered a two-phase model to discuss the dispersion phenomena of a tracer substance in respect of three effective transport coefficients, namely, the fraction of solute left in the fluid phase, the apparent convection velocity, and the dispersion coefficient. For oscillatory flow through an annular region, Sarkar and Jayaraman[16] studied the dispersion of a tracer in the presence of irreversible reaction at the boundary. A number of studies on solute dispersion in Newtonian fluid through a tube/channel were carried out by considering both the reversible and irreversible boundary reactions (cf. Ng,[17] Ng and Rudraiah,[18] and Mazumder and Paul[19]) and by considering a porous tube/channel (cf. Griffiths *et al.*,[20] Dejam *et al.*,[21] and Kou and Dejam[22]).

A state-of-the-art model for transport in blood vessels is indispensable for a better understanding of normal physiological function and interpretation of the findings obtained from experiments. This dispersion model is applicable for transport of solutes in blood vessels and of soluble gases in the airways of the lung (cf. Phillips *et al.*[1]). To represent the non-Newtonian behavior of the fluid, Casson model has received much attention than other non-Newtonian models present in the literature. At a low shear rate, the Casson fluid model could be well representative of blood when it flows through a vessel of smaller diameter in the presence of hematocrits, anticoagulants, etc. (cf. Charm and Kurland,[23] Blair and Spanner,[24] and MacDonald[25]). Sharp[26] analytically determined the same proportionalities as in Taylor's theory by considering various fluid rheologies like Casson model, Power-law model, and Bringham fluid. Dash *et al.*[27] determined the flow characteristics of Casson fluid for practical applications in the study of coronary artery disease. Later, they[28] described the solute dispersion process in Casson fluid flow under the effect of variation in yield stress, using generalized dispersion model. Considering both tube and channel flows of Casson fluid, Nagarani *et al.*[29] investigated the effect of wall absorption parameter and yield stress on solute dispersion. Due to its significant application in physiological and industrial problems, several researchers (cf. Nagarani *et al.*,[30] Shaw *et al.*,[31] Rana and Murthy,[32,33] Debnath *et al.*,[34–37] and Roy *et al.*[38–40]) carried out extensive studies on dispersion of solute in Casson fluid flow. Abbas *et al.*[41] analyzed the flow phenomena of Casson fluid flow between parallel disks under different motion conditions of disk. Later, Abbas *et al.*[42] deliberated the impact of thermal radiation on the peristaltic transport of a Casson fluid through an inclined tube. In the presence of thermal radiation, the effect of variable viscosity on Casson fluid flow in expanding/contracting channel with porous walls examined by Rafiq *et al.*[43] Rana and Murthy[44,45] and Rana and Liao[46] have considered various non-Newtonian models to study the unsteady solute dispersion in the presence of wall absorption. Sarifuddin *et al.*[47,48] discussed the flow characteristics of fluid and mass transport in the case of flow past an atherosclerotic vessel. To investigate the temperature and the concentration dispersion, Reddy *et al.*[49] assumed nanofluid flows in a stenotic artery. Very recently, Das *et al.*[6] extensively studied the dispersion of solute in Casson fluid flow in a two-phase stenotic system having a first-order irreversible reaction at the interface. Effect of porous vessel wall on solute dispersion process in two-fluid model of blood flow was discussed by Tiwari *et al.*[50] and Shah *et al.*[51] Since the majority of computational models tend to neglect the transient behavior of the non-Newtonian fluid past a stenosis and/or the inclusion of the tissue domain, these models are likely to be under-or over-estimating solute uptake and redistribution in arterial tissue.

Computational modeling and numerical simulation have risen as a fundamental tool in the investigation of targeted drug delivery, helping to address some of the limitations of expensive and even extremely variable experimental tests. It has enhanced the understanding of the dispersion of the solute and its subsequent uptake by the absorbing wall, and finally its transport into the arterial tissue. The majority of the above works was performed considering the tubular geometrical model with linear boundary and restricted themselves to analyze the solute dispersion in the fluid phase of the tube only. In the present investigation, we consider an idealized cosine-shaped stenotic tube as a computational domain consisting of a fluid phase and a wall (tissue) phase. The solute is injected at a point uniformly distributed over the cross section of the lumen. We provide an extensive computational study of unsteady solute dispersion in the transient non-Newtonian flow of blood in a stenosed artery and in the arterial wall, in general,

and we perform a large scale computation to elucidate the effect of non-Newtonian rheology and the severity of the stenosis on the transport coefficients and the spatiotemporal pattern of the dispersion in the lumen as well as in the tissue. The discretized governing equations representing the unsteady solute and momentum transport are solved numerically using the Marker and Cell (MAC) method and the immersed boundary method (IBM) in an irregular domain (cf. Peskin[52]). The primary objective of the present study is to estimate the effects of non-Newtonian rheology, absorption parameter, and severity of the stenosis on various time-dependent factors like the fraction of solute remaining in the fluid phase, the apparent convection velocity, the dispersion coefficient, the spatiotemporal concentration, and the axial mean concentration. The novelty of the present study is the consideration of Casson model and the dispersion of the solute in the tissue in general, and the choice of solute administration at a point uniformly distributed over a cross section, which closely resembles the physiological situation concerning intravenous drug delivery.

## II. MATHEMATICAL FORMULATION

### A. Geometry of the stenosed artery

The geometry of the arterial segment having a cosine-shaped axisymmetric stenosis in its lumen[53,54] is of the form

$$R_i(z) = \begin{cases} 1 - \dfrac{\xi}{2r_0}\left[1 + \cos\left\{\dfrac{\pi z}{z_0}\right\}\right] & -z_0 \le z \le z_0, \\ 1 & \text{otherwise}, \end{cases} \tag{1}$$

where $z_0$ is the half-length and $\xi$ is the maximum height of the stenosis (cf. Fig. 1). The lumen is surrounded by a tissue layer of thickness $[R_p - R_i(z)]$ where the maximum thickness occurs at $z = 0$.

### B. Momentum transport equations

A two-dimensional unsteady flow of Casson fluid under axisymmetric conditions in cylindrical polar coordinates system $(r, \theta, z)$ may be written in a dimensional form as

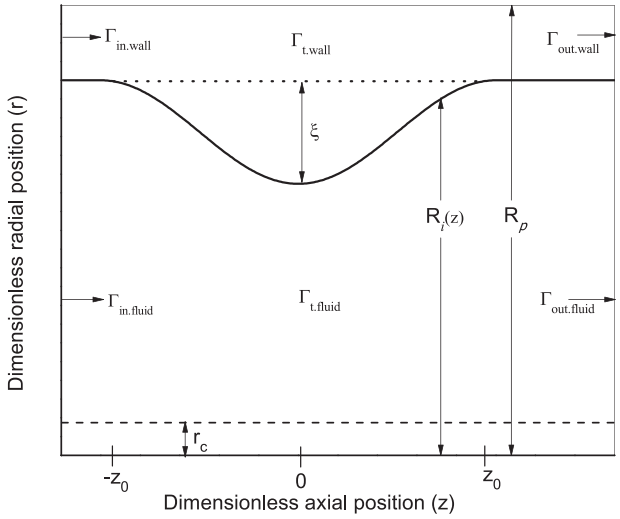


**FIG. 1.** Schematic diagram of the cosine-shaped stenosis model with 48% area occlusion.

$$\frac{\partial u_z}{\partial t} + u_r\frac{\partial u_z}{\partial r} + u_z\frac{\partial u_z}{\partial z} = -\frac{1}{\rho}\frac{\partial p}{\partial z} - \frac{1}{\rho}\left(\frac{\partial \tau_{rz}}{\partial r} + \frac{\partial \tau_{zz}}{\partial z} + \frac{\tau_{rz}}{r}\right), \tag{2}$$

$$\frac{\partial u_r}{\partial t} + u_r\frac{\partial u_r}{\partial r} + u_z\frac{\partial u_r}{\partial z} = -\frac{1}{\rho}\frac{\partial p}{\partial r} - \frac{1}{\rho}\left(\frac{\partial \tau_{rr}}{\partial r} + \frac{\partial \tau_{rz}}{\partial z} + \frac{\tau_{rr}}{r} - \frac{\tau_{\theta\theta}}{r}\right), \tag{3}$$

and

$$r\frac{\partial u_z}{\partial z} + \frac{\partial (r u_r)}{\partial r} = 0. \tag{4}$$

The rheological equation[55] considering an isotropic, incompressible flow of a Casson fluid can be written as

$$\tau_{ij} = 2\mu(J_2)\phi_{ij}, \tag{5}$$

where

$$\mu(J_2) = \left[2^{-\frac{1}{2}}\tau_y^{\frac{1}{2}} + (\eta^2 J_2)^{\frac{1}{4}}\right]^2 J_2^{-\frac{1}{2}},$$

$$J_2 = \left[2\left\{\left(\frac{\partial u_r}{\partial r}\right)^2 + \left(\frac{u_r}{r}\right)^2 + \left(\frac{\partial u_z}{\partial z}\right)^2\right\} + \left(\frac{\partial u_r}{\partial z} + \frac{\partial u_z}{\partial r}\right)^2\right].$$

The mathematical form of flow criteria for Casson model is given by

$$\phi_{ij} = \begin{cases} 0, & J_2^* < \tau_y^2, \\ \dfrac{1}{2\mu(J_2)}\tau_{ij}, & J_2^* \ge \tau_y^2. \end{cases} \tag{6}$$

The dimensionless quantities $u_z(t, z, r)$ and $u_r(t, z, r)$ are the axial and the radial components of velocity conponents, respectively, scaled with respect to the centerline velocity in a Poiseuille flow $U_0$. The dimensionless radial coordinate $(r)$ and the axial coordinate $(z)$ are normalized with respect to the upstream radius of the lumen $r_0$ and $Pe_f r_0$, respectively. The dimensionless shear stress $(\tau_{ij})$, the Reynolds number $(Re)$, the dimensionless pressure $(p)$, and the Peclet number for the fluid phase can be written, respectively, as

$$\tau_{ij} = \frac{\tau'_{ij} r_0}{\eta U_0}, \quad Re = \frac{\rho U_0 r_0}{\eta}, \quad p = \frac{p'}{\rho U_0^2}, \quad Pe_f = \frac{r_0 U_0}{D_f}.$$

Here, $D_f$, $\mu(J_2)$, $J_2 (= \frac{1}{2}\phi_{ij}\phi_{ij})$, $\phi_{ij}$, and $J_2^* (= \frac{1}{2}\tau_{ij}\tau_{ij})$ stand for the fluid phase diffusion coefficient, apparent viscosity, the rate of strain tensor invariant, rate of strain tensor, and the second invariant of the stress tensor, respectively. The parameters $\tau_y$, $\eta$, and $\rho$ represent the yield stress, the viscosity coefficient, and the fluid density, respectively. The derivation of the governing equations (2)–(4) is given in the Appendix.

The governing equations in a non-dimensional form can be written as

$$\frac{1}{Pe_f}\frac{\partial u_z}{\partial t} + \frac{\partial (u_z u_r)}{\partial r} + \frac{1}{Pe_f}\frac{\partial (u_z^2)}{\partial z} + \frac{(u_z u_r)}{r} = -\frac{1}{Pe_f}\frac{\partial p}{\partial z} - \frac{1}{Re}\left[\frac{\partial \tau_{rz}}{\partial r} + \frac{1}{Pe_f}\frac{\partial \tau_{zz}}{\partial z} + \frac{\tau_{rz}}{r}\right], \tag{7}$$

$$\frac{1}{Pe_f}\frac{\partial u_r}{\partial t}+\frac{\partial(u_r^2)}{\partial r}+\frac{1}{Pe_f}\frac{\partial(u_z u_r)}{\partial z}+\frac{(u_r^2)}{r} = -\frac{\partial p}{\partial r}-\frac{1}{Re}\left[\frac{\partial \tau_{rr}}{\partial r}+\frac{1}{Pe_f}\frac{\partial \tau_{rz}}{\partial z}+\frac{\tau_{rr}-\tau_{\theta\theta}}{r}\right], \tag{8}$$

$$\frac{r}{Pe_f}\frac{\partial u_z}{\partial z}+\frac{\partial(ru_r)}{\partial r}=0, \tag{9}$$

where

$$\tau_{zz}=-2\mu(J_2)\left(\frac{1}{Pe_f}\frac{\partial u_z}{\partial z}\right),\quad \tau_{rr}=-2\mu(J_2)\left(\frac{\partial u_r}{\partial r}\right),$$
$$\tau_{\theta\theta}=-2\mu(J_2)\left(\frac{u_r}{r}\right),\quad \tau_{rz}=-\mu(J_2)\left(\frac{\partial u_z}{\partial r}+\frac{1}{Pe_f}\frac{\partial u_r}{\partial z}\right),$$

with

$$\mu(J_2)=\left[2^{-\frac{1}{2}}\tau_y^{\frac{1}{2}}+J_2^{\frac{1}{4}}\right]^2 J_2^{-\frac{1}{2}},$$
$$J_2=\left[2\left\{\left(\frac{\partial u_r}{\partial r}\right)^2+\left(\frac{u_r}{r}\right)^2+\left(\frac{1}{Pe_f}\frac{\partial u_z}{\partial z}\right)^2\right\}+\left(\frac{1}{Pe_f}\frac{\partial u_r}{\partial z}+\frac{\partial u_z}{\partial r}\right)^2\right].$$

#### 1. Initial and boundary conditions for velocity

Initially, it is assumed that the system is at rest except a fully developed flow of Casson fluid at the inlet whose mathematical form may be as[29,55]

$$u_z(t,z,r)|_{z=\Gamma_{in,fluid}}=\begin{cases}\left[(1-r^2)-\frac{8}{3}r_c^{\frac{1}{2}}(1-r^{\frac{3}{2}})+2r_c(1-r)\right], & \text{for } r_c\le r<R_i(z)|_{z=\Gamma_{in,fluid}},\\ \left[1-\frac{8}{3}r_c^{\frac{1}{2}}+2r_c-\frac{1}{3}r_c^2\right], & \text{for } 0\le r\le r_c,\end{cases} \tag{10}$$

and

$$u_r(t,z,r)|_{z=\Gamma_{in,fluid}}=0,\quad \text{for } 0\le r<R_i(z)|_{z=\Gamma_{in,fluid}}, \tag{11}$$

where $r_c\left(=\frac{\tau_y}{2}\right)$ stands for the radius of the plug region.

At the lumen-tissue interface, the usual no-slip boundary condition is given by

$$u_z(t,z,r)=0=u_r(t,z,r),\quad \text{at } r=R_i(z). \tag{12}$$

The axial symmetry condition at the centerline is given by

$$\frac{\partial u_z}{\partial r}(t,z,r)=0=u_r(t,z,r),\quad \text{at } r=0. \tag{13}$$

At the downstream, the flow is left free which is mathematically written as

$$\frac{\partial u_z}{\partial z}(t,z,r)=0=\frac{\partial u_r}{\partial z}(t,z,r),\quad \text{on } \Gamma_{out,fluid}. \tag{14}$$

### C. Solute transport equations

In the presence of non-Newtonian Casson fluid flow, the transportation of solute through a stenotic tube in the fluid phase and wall phase due to solute exchange between two phases can be represented by the convection-diffusion equations whose mathematical expressions in dimensionless forms in the cylindrical polar coordinate system $(r,\theta,z)$ can be written as (cf. Phillips *et al.*[1])

$$\frac{\partial C_f}{\partial t}+Pe_f u_r\frac{\partial C_f}{\partial r}+u_z\frac{\partial C_f}{\partial z}=\left(\frac{\partial^2 C_f}{\partial r^2}+\frac{1}{r}\frac{\partial C_f}{\partial r}+\frac{1}{Pe_f^2}\frac{\partial^2 C_f}{\partial z^2}\right) \tag{15}$$

and

$$\frac{\partial C_w}{\partial t}=\lambda\left(\frac{\partial^2 C_w}{\partial r^2}+\frac{1}{r}\frac{\partial C_w}{\partial r}+\frac{1}{Pe_f^2}\frac{\partial^2 C_w}{\partial z^2}\right), \tag{16}$$

where the dimensionless parameter $\lambda\left(=\frac{D_w}{D_f}\right)$ be the ratio of the diffusion coefficient $(D_w)$ in the wall phase and the diffusion coefficient $(D_f)$ in the fluid phase. The solute concentrations in the fluid phase $(C_f)$ and in the wall phase $(C_w)$ both are scaled with $\frac{M}{\pi Pe_f r_0^3}$, where $M$ is the total mass initially present.[1]

#### 1. Initial and boundary conditions for solute

Initially at $z=0$, an injected solute is uniformly distributed over the cross section inside the lumen, and therefore, the initial condition of concentration can be written mathematically in a dimensionless form as[1]

$$\begin{cases}C_f(t,z,r)|_{t=0,z=0}=\delta(z)H(1-r), & \text{for } r\le R_i(z) \text{ on}\Gamma_{t.fluid},\\ C_w(t,z,r)|_{t=0}=0, & \text{for } r>R_i(z) \text{ on}\Gamma_{t.wall},\end{cases} \tag{17}$$

where $\delta$ is the Dirac delta function and $H$ is the Heaviside function.

The conditions for concentration at the proximal and distal ends for the luminal and tissue domains may be taken as

$$\begin{cases}C_f=0, & \text{as } z\to\pm\infty,\\ \frac{\partial C_w}{\partial z}(t,z,r)=0, & \text{as } z\to\pm\infty.\end{cases} \tag{18}$$

Moreover, at the centerline, the condition for solute concentration is given by

$$\frac{\partial C_f}{\partial r}(t,z,r)=0, \quad \text{at } r=0. \tag{19}$$

At the fluid-wall interface, continuity of concentration and solute flux between fluid phase and wall phase has been taken in the dimensionless mathematical form as[1]

$$\begin{cases} C_w(t,z,r)=\beta C_f(t,z,r), & \text{on } R_i(z), \\ \lambda\dfrac{\partial C_w}{\partial n}(t,z,r)=\dfrac{\partial C_f}{\partial n}(t,z,r), & \text{on } R_i(z), \end{cases} \tag{20}$$

where $\beta$ is the ratio of wall phase concentration to fluid phase concentration at equilibrium, and the dimensionless parameter $\kappa\left(=\lambda^{\frac{1}{2}}\beta\right)$ represents the absorption parameter.

At the perivascular wall, a perfectly absorbing condition may be taken as

$$C_w(t,z,r)=0, \quad \text{at } r=R_p. \tag{21}$$

### D. Determination of transport coefficients

Following Davidson and Schroter,[56] let us determine the transport coefficient in the fluid and wall phases as

$$\langle C(t)\rangle=\frac{2}{R_p^2}\int_{-\infty}^{\infty}\int_0^{R_p} rC(t,z,r)\,dr\,dz, \tag{22}$$

where

$$\begin{cases} C(t,z,r)=C_f(t,z,r), & \text{for } r\le R_i(z), \\ C(t,z,r)=C_w(t,z,r), & \text{for } r>R_i(z). \end{cases} \tag{23}$$

The above integral can be split over the fluid phase and the wall phase with same normalization.

The fraction of solute remaining in fluid phase can be termed as

$$q_f(t)=\int_{-\infty}^{\infty}\frac{\int_0^{R_i(z)} rC_f(t,z,r)\,dr}{\int_0^{R_i(z)} r\,dr}\,dz. \tag{24}$$

The apparent convection velocity of solute is $U_0u(t)$, where

$$u(t)=\frac{d}{dt}\left(\frac{\langle zC(t)\rangle}{\langle C(t)\rangle}\right). \tag{25}$$

The dispersion coefficient $D_fk(t)$ is defined as half the rate of change of axial variance of solute, where

$$k(t)=\frac{1}{2}Pe_f^2\frac{d}{dt}\left[\frac{\langle z^2C(t)\rangle}{\langle C(t)\rangle}-\left(\frac{\langle zC(t)\rangle}{\langle C(t)\rangle}\right)^2\right]. \tag{26}$$

## III. METHOD OF SOLUTION

### A. The MAC methodology

The Marker and Cell (MAC) method has been adopted to simulate for the flow-field and solute concentration in interior cells from the momentum equations and convection-diffusion equations, respectively, using the prescribed initial and boundary conditions. The velocity, pressure, and concentration components are computed at different positions of the MAC cell as depicted in Fig. 2. The first-order forward difference formula is applied for the time derivatives terms, whereas a hybrid second-order upwinding difference scheme is considered for the convection terms. The diffusive terms are discretized using the second-order accurate three-point central difference formula.

The discretized version of the continuity equation at $(i,j)^{th}$ cell is of the form

$$\frac{r_j}{Pe_f}\left(\frac{u^n_{z\left(i+\frac{1}{2},j\right)}-u^n_{z\left(i-\frac{1}{2},j\right)}}{\delta z}\right)+\left(\frac{r_{j+\frac{1}{2}}u^n_{r\left(i,j+\frac{1}{2}\right)}-r_{j-\frac{1}{2}}u^n_{r\left(i,j-\frac{1}{2}\right)}}{\delta r}\right)=0, \tag{27}$$

where the axial and the radial velocity components are discretized as $u_z(t,z,r)=u_z(n\delta t,i\delta z,j\delta r)=u^n_{z(i,j)}$ and $u_r(t,z,r)=u_r(n\delta t,i\delta z,j\delta r)=u^n_{r(i,j)}$, respectively, in which $n$ stands for time direction and $\delta t,\delta z,\delta r$ as time increment, length increment, and breadth increment, respectively.

To determine the pressure component at each cell from the pressure equation, derived from the discretized momentum equations, the successive-over-relaxation (S.O.R.) method is applied with the over-relaxation parameter as 1.2, and the intermediate pressure-field is deduced using the velocity field already obtained. The divergence of the velocity-field is calculated throughout the domain and checked for its maximum divergence value. If this value exceeds the tolerance limit, then the pressure-velocity correction scheme is applied as described in Sec. III C. The solute concentrations in the fluid phase and wall phase are explicitly determined from the discretized version of Eqs. (15) and (16), respectively.

### B. The immersed boundary method

As rectilinear grids are not conformed with complex geometry, to estimate the values of the velocity, pressure, and concentration at the intercepted cells (the cell where some grid points lie inside the fluid domain and some points lie in the wall domain), the IBM is applied in

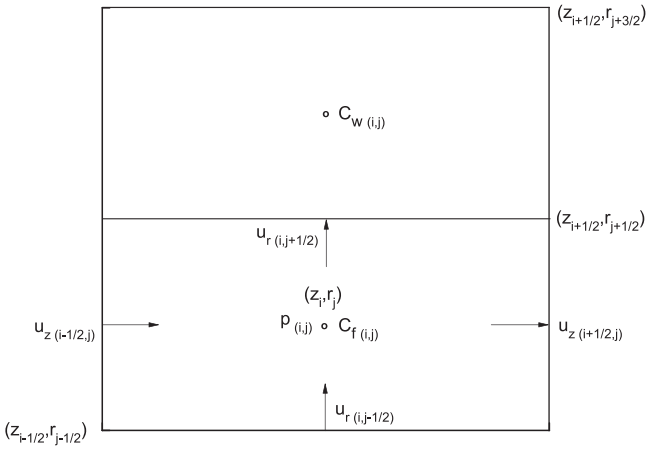


**FIG. 2.** A typical MAC cell.

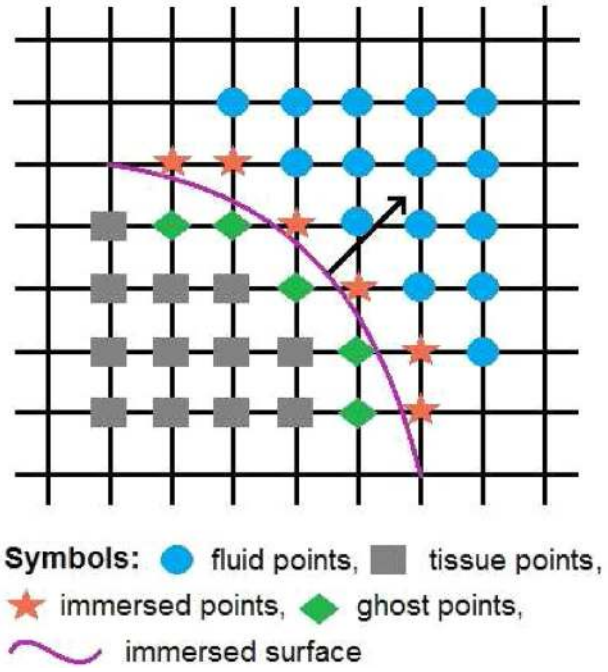


**FIG. 3.** Depiction of interpolation scheme for immersed boundary method.

staggered grids. In the present analysis, a direct forcing approach has been considered satisfying the no-slip and other prescribed boundary conditions and determined the desired quantities at the vicinity of the interfaces.[57] Before the implementation of the IBM, it is necessary to search whether a cell near the boundary is situated in the fluid domain or in the wall domain or intercepted between the fluid and the wall domains (cf. Fig. 3). This process is called "Cell tagging" and an efficient search algorithm is made use of for this purpose.[6,57]

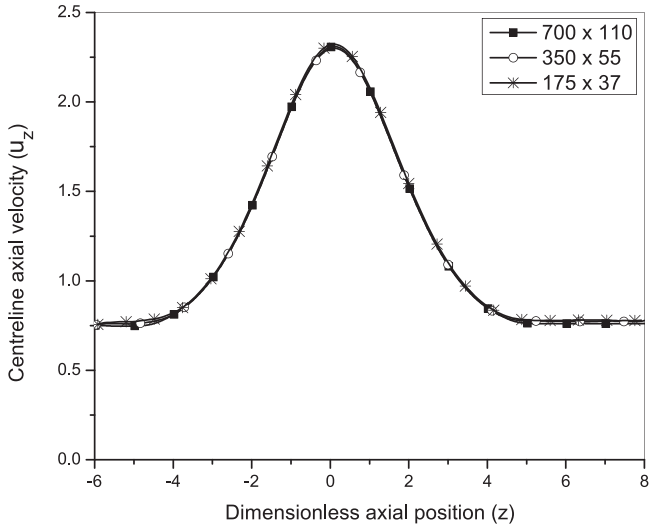


**FIG. 4.** Grid independent study. Centerline velocity for different grid sizes (64% severity of the stenosis, $Re = 100$, $Pe_f = 20$, and $\tau_y = 0.02$).

The curved interface is recognized by using a set of connected points in the background of a structured mesh. The location of the grid point in the wall/fluid domain is governed by the value of the dot product of the position vector of grid point ($\vec{g}$) and surface normal vector ($\hat{n}$). The grid point is located at fluid phase for $\vec{g} \cdot \hat{n} \geq 0$, whereas if $\vec{g} \cdot \hat{n} < 0$, then grid point lies in the wall phase. At the "intercepted cells," some vertices (nodes) are in the fluid phase (called "immersed nodes") and some are outside the fluid phase (called "ghost nodes") (cf. Fig. 3). A similar approach has been applied for the cells in the wall phase. This cell tagging procedure is implemented throughout the computational domain at all the staggered grids. Thereafter, an interpolation scheme is applied successfully to determine the velocity profile, pressure, and concentration at immersed and ghost nodes.

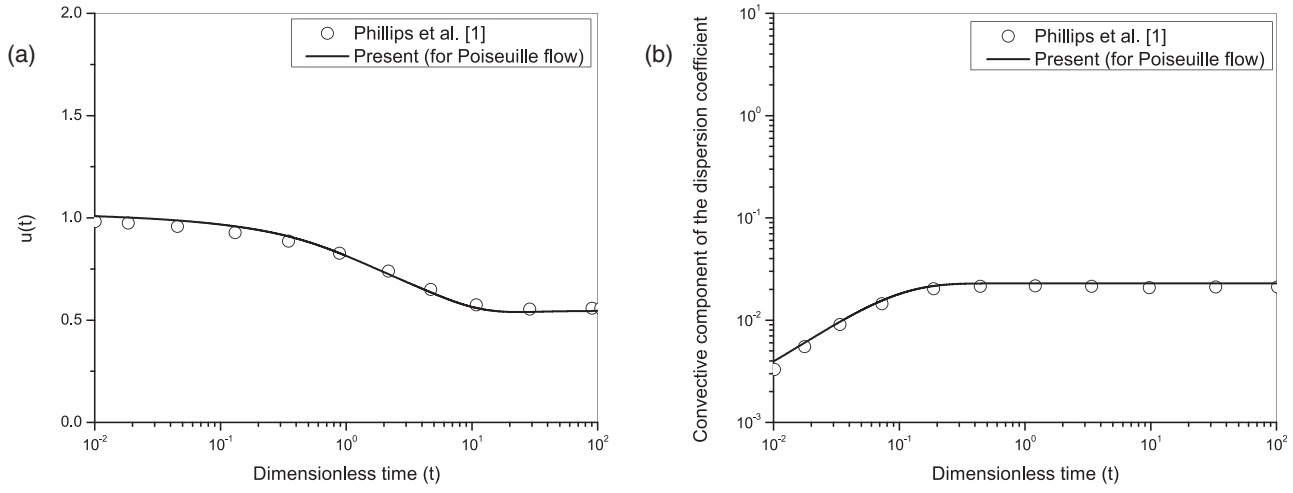


**FIG. 5.** Model validation: (a) the apparent convection velocity of solute based on averages over both phases for $\kappa = 0.1$ and (b) the convective component of the dispersion coefficient based on averages over both phases for $\kappa = 0$.

**TABLE I.** Baseline values of involved parameters.

| Description | Parameters | Values | References |
|---|---|---|---|
| Centerline velocity | | | |
| In a Poiseuille flow (cm/s) | $U_0$ | 14.0 | 64 |
| Upstream radius (cm) | $r_0$ | 0.02 | 33 and 65 |
| Fluid density (g m/cm$^3$) | $\rho$ | 1.05 | 53 |
| Yield stress (dyn/cm$^2$) | $\tau_y$ | $(0-0.2)$ | 28 |
| Reynolds number | $Re$ | $(20-1000)$ | 53 |
| Wall absorption parameter | $\kappa$ | $(0.001-10)$ | 1 |
| Dimensionless parameter | $\lambda$ | $10^{-4}$ | 1 |

The quadratic polynomial of the form $f(n) = an^2 + bn + c$ is considered to maintain the overall-second order accuracy of the solution algorithm and computed the value of all the desired variables at the cut-cell grid points by performing interpolation and extrapolation,[57,58] where $n$ represents the coordinate value along the surface normal direction. Consider two points along the normal direction where $f$ is known and one point at the interface where $n = 0$ such that the value of $f$ satisfies the boundary conditions. With the help of the function values at these three points, the unknown coefficients $a$, $b$, and $c$ are determined.

### C. Pressure and velocity correction

While calculating pressure at each cell center, the number of iteration of the S.O.R. scheme is limited to 10 to save computational cost.

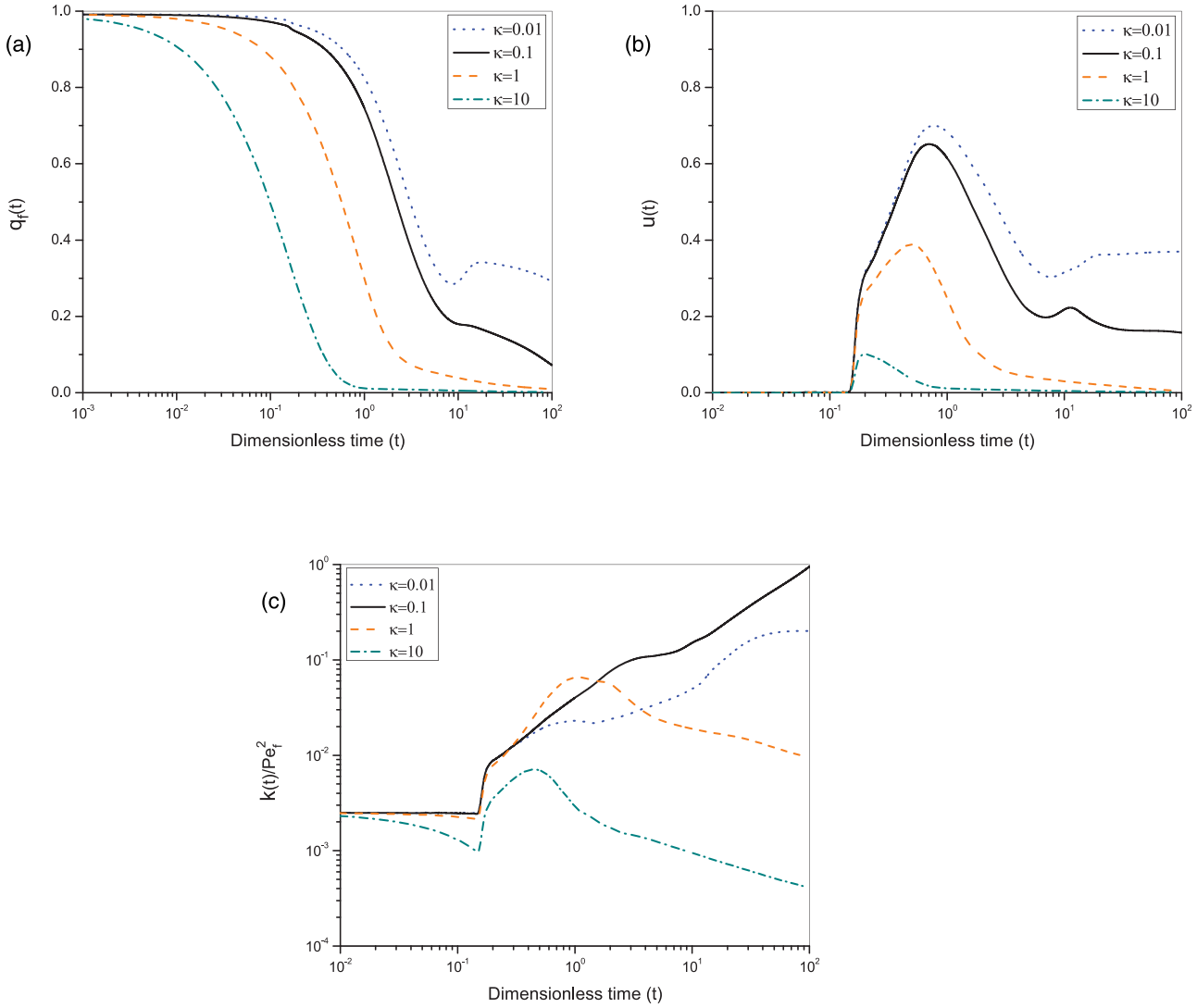


**FIG. 6.** Variation of transport coefficients for different values of the wall absorption parameter $\kappa$ (48% severity of the stenosis, $Re = 50$, $Pe_f = 20$, and $\tau_y = 0.02$). (a) The fraction of solute remaining in the fluid phase. (b) The apparent convection velocity based on averages over both phases. (c) The dispersion coefficient based on average over both phases.

The velocity-field obtained using these inaccurate pressure values may not satisfy the continuity equation, in general, and hence this necessitates a corrector stage.

The pressure correction formula is of the form

$$p^{n}_{(i,j)} = p^{\star}_{(i,j)} + \omega \delta p_{(i,j)}, \tag{28}$$

with

$$\delta p_{(i,j)} = -\left[\frac{Div^{\star}_{(i,j)}}{\delta t\left(\frac{2r_j}{Pe_f \delta z^2} + \frac{Pe_f\, r_{j-1/2}}{\delta r^2} + \frac{Pe_f\, r_{j+1/2}}{\delta r^2}\right)}\right],$$

where $p^{\star}_{(i,j)}$ is the obtained pressure from the pressure equation, $\omega\,(\leq 0.5)$ is the relaxation parameter for S.O.R scheme, and $Div^{\star}_{(i,j)}$ stands for divergence of the velocity-field at $(i,j)^{th}$ cell derived after solving the pressure equation.

The axial and radial velocity correction formulas are[47]

$$\begin{cases} u^{n+1}_{z\left(i+\frac{1}{2},j\right)} = u^{\star}_{z\left(i+\frac{1}{2},j\right)} + \dfrac{\delta t \delta p_{(i,j)}}{\delta z}, \\ u^{n+1}_{z\left(i-\frac{1}{2},j\right)} = u^{\star}_{z\left(i-\frac{1}{2},j\right)} - \dfrac{\delta t \delta p_{(i,j)}}{\delta z}, \\ u^{n+1}_{r\left(i,j+\frac{1}{2}\right)} = u^{\star}_{r\left(i,j+\frac{1}{2}\right)} + \dfrac{Pe_f \delta t \delta p_{(i,j)}}{\delta r}, \\ u^{n+1}_{r\left(i,j-\frac{1}{2}\right)} = u^{\star}_{r\left(i,j-\frac{1}{2}\right)} - \dfrac{Pe_f \delta t \delta p_{(i,j)}}{\delta r}, \end{cases} \tag{29}$$

where $u^{\star}_{z\left(i+\frac{1}{2},j\right)}$, $u^{\star}_{z\left(i-\frac{1}{2},j\right)}$, $u^{\star}_{r\left(i,j+\frac{1}{2}\right)}$, and $u^{\star}_{r\left(i,j-\frac{1}{2}\right)}$ represent the updated velocity-field.

### D. Numerical stability

To obtain a stable numerical solution, we adopted the following time stepping schemes. Welch *et al.*[59] and Hirt[60] suggested stability criteria consisting of Reynolds number and can be applied for MAC methodology directly for a suitable time stepping ($\delta t_1$).

Another elegant time measuring criteria recommended by Markham and Proctor[61] in which at any given time step ($\delta t_2$), no fluid particle should pass more than one cell.

On account of solute diffusivity and dimensions of the control volume, Courant–Friedrichs–Lewy stability criteria[62] provided the time stepping ($\delta t_3$).

Moreover, considering all the criteria, we adopted a suitable time stepping ($\delta t$), which is the minimum of all above three criteria. For details of mathematical expression of time stepping, interested readers are referred to Sarifuddin and Mandal.[63]

### E. Grid independence study and model validation

To verify the correctness of the computational code and error associated with the grid sizes used, a grid independence study is performed for centerline axial velocity at different grid sizes (relatively coarse and finer) as shown in Fig. 4. It is noticeable that all three velocity profiles are almost overlapped with one another establishing the correctness of the code at grid sizes used.

In order to validate our results, some comparisons have been made with the results of Phillips *et al.*[1] It may be recalled that Phillips *et al.*[1] studied the time-dependent dispersion of solute in both fluid and wall phases in the presence of fully developed Poiseuille flow while our model demands appreciable extension over that with some additional assumptions, namely, the transient flow of non-Newtonian fluid (Casson fluid) and the presence of stenosis in which the solute is injected at the throat of the stenosis. In a bid to validate our results, we reduce our model to that of Phillips *et al.*[1] and determine the apparent convection velocity and the convective component of the dispersion coefficient both based on averages over both phases shows excellent agreement as exhibited in Figs. 5(a) and 5(b).

## IV. RESULTS AND DISCUSSION

To investigate the dispersion of solute in a two-phase domain such as lumen and tissue region, an unsteady analysis of mass and momentum transport has been carried out in which the fluid is represented by a non-Newtonian Casson model. The stenotic tube with boundary absorption and two-dimensional flow are considered in this study. The effect of the wall absorption parameter ($\kappa$), yield stress ($\tau_y$), and the severity of the stenosis ($\xi$) on the solute dispersion process has been analyzed. The dispersion phenomena of the solute in both lumen and tissue regions are explored numerically by applying leveraging the Marker and Cell (MAC) method and the IBM in staggered grids formulation. With the time step obtained in Sec. III D and $\Delta r = 0.02, \Delta z = 0.04$, we determine the transport coefficients for larger time by extending the domain progressively in the downstream to $-6 \leq z \leq 8$ to provide enough room for the solute to move downstream and to ensure that no solute particle leave the domain.[18] The steady state is achieved when the maximum divergence of the velocity field is less than $10^{-12}$ and for concentration, the tolerance is less than $10^{-5}$ in the absolute sense. The plausible values of the parameters involved in the computation of the desired quantities having major physiological significance are given in Table I. The stability of our numerical schemes has been discussed and the correctness of the

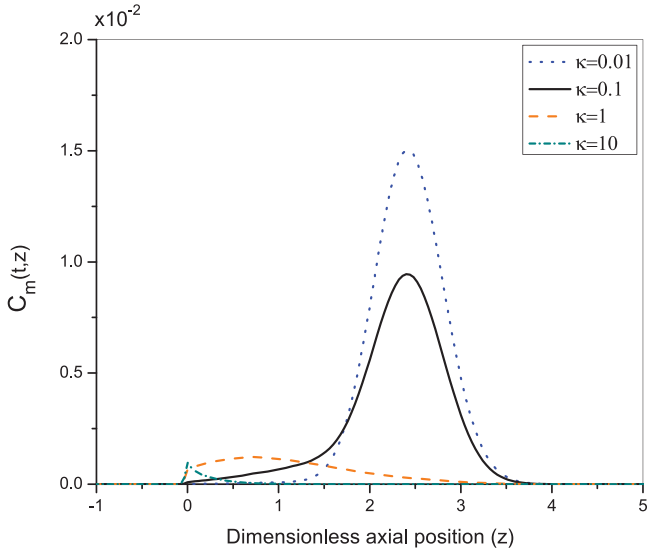


**FIG. 7.** The variation of axial mean concentration in fluid phase averages over luminal cross section for different values of the wall absorption parameter $\kappa$ at $t = 5$ (48% severity of the stenosis, $Re = 50$, $Pe_f = 20$, and $\tau_y = 0.02$).

computational code is justified in this analysis. In addition, to check the accuracy of the present investigation, our obtained results are compared with the existing results in some special cases and found to be in good agreement.

### A. Effect of wall absorption parameter $\kappa$

One of the key parameters that controls the solute transfer between two phases is the wall absorption parameter $\kappa$. Its effects on three time-dependent transport coefficients are displayed in Fig. 6 in logarithmic scale. It is noticed that the effects of wall absorption parameter on the time-dependent transport coefficients are nonlinear. These nonlinear effects are elaborately discussed in this study. The fraction of solute remaining in the fluid phase $[q_f(t)]$ strongly relies on time $t$ and $\kappa$, and it is shown in Fig. 6(a). It is observed that at small time for small values $\kappa$, there is no significant change in $q_f(t)$ but at large time, $q_f(t)$ decreases, and at very large time (after $t \sim 10$), it approaches to a constant value. However, for large values of $\kappa$ at small time, $q_f(t)$ starts to decrease significantly and at large time, it reaches early to a constant value. The physical significance of this

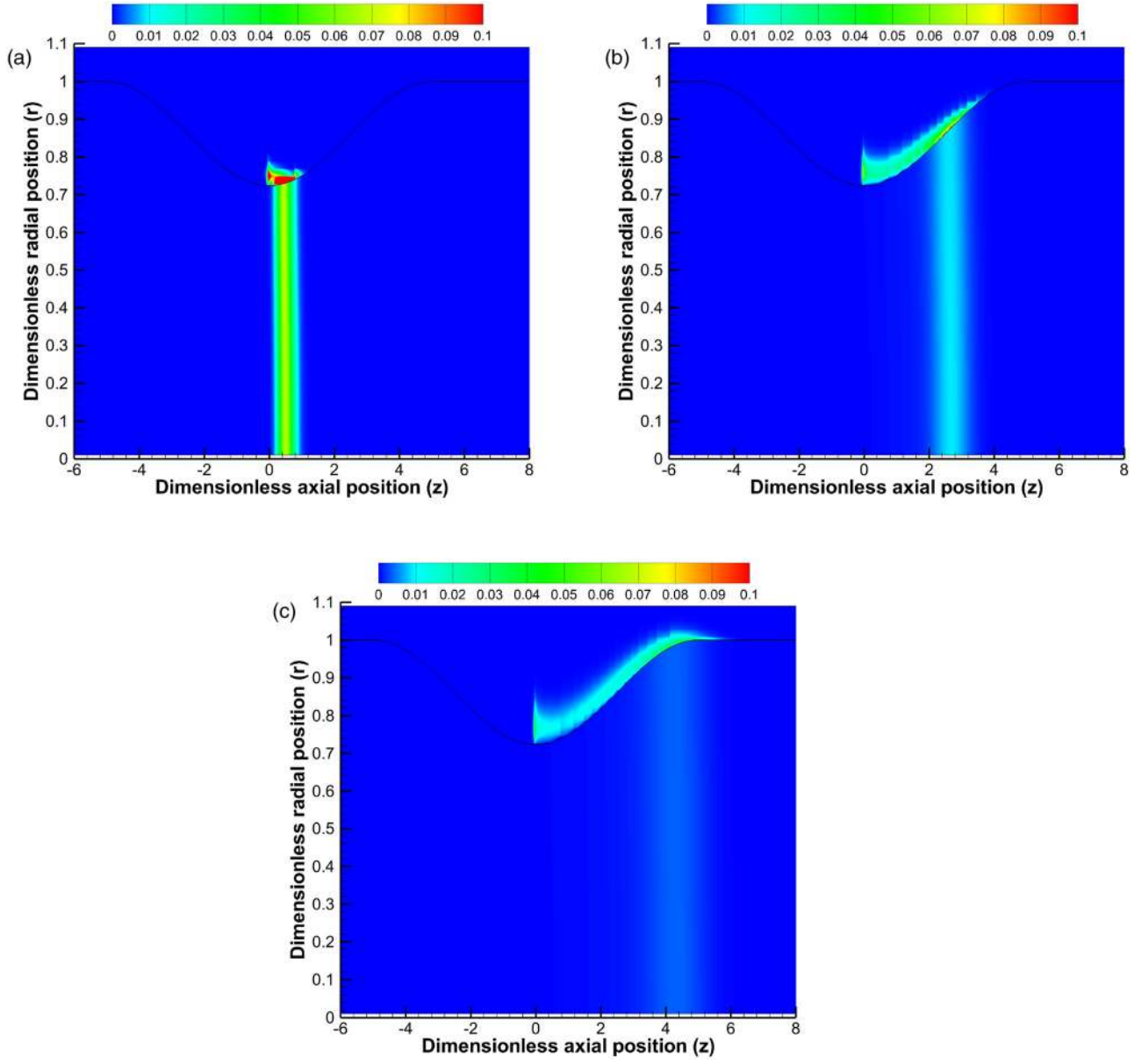


**FIG. 8.** Spatiotemporal variation of solute concentration for different times (48% severity of the stenosis, $Re = 50$, $Pe_f = 20$, $\kappa = 0.1$, and $\tau_y = 0.02$). (a) $t = 1$, (b) $t = 5$, and (c) $t = 10$.

phenomenon is that small values of $\kappa$ lead to low absorption rate at the tube wall and due to this reason, at small time, very less amount of solute is transported from the center of the tube to the wall region for conducting the absorption. So, more amount of solute is present in the fluid phase at small time. However, at large time, the convective and diffusive transportation of the solute becomes more effective in the system. For this reason, the solute decreases in the fluid phase and transported to the wall region. Now at very large time, an equilibrium state occurs between the absorption at the tube wall and the diffusive transport from the center of the tube to wall region. For small values of $\kappa$, owing to the presence of comparatively higher amount of solute substance in the fluid phase, it takes a larger time to achieve an equilibrium state. That means sufficient amount of solute retains in the fluid phase for a more extended period in the case of lower values of $\kappa$ and it is getting enough time to reach an equilibrium stage. However, for large values of $\kappa$, the rate of absorption at the tube wall becomes more. Due to this, more amount of solute is transported to the tube wall region. So, very less amount is present in the fluid phase. In addition, the convective and diffusive transportation of the solute enhances the depletion of the solute in the fluid phase. Therefore, at large time, an equilibrium state is reached, i.e., the depletion becomes in stable condition. Hence, for large values of $\kappa$, less time is required to reach the equilibrium state. That means most of the solute substance absorbed quickly for higher values of $\kappa$ and does not get enough extent to attain the equilibrium stage. Also, it is evident from Fig. 6(a) that $q_f(t)$ decreases as $\kappa$ increases. The physical clarification is that as $\kappa$ increases

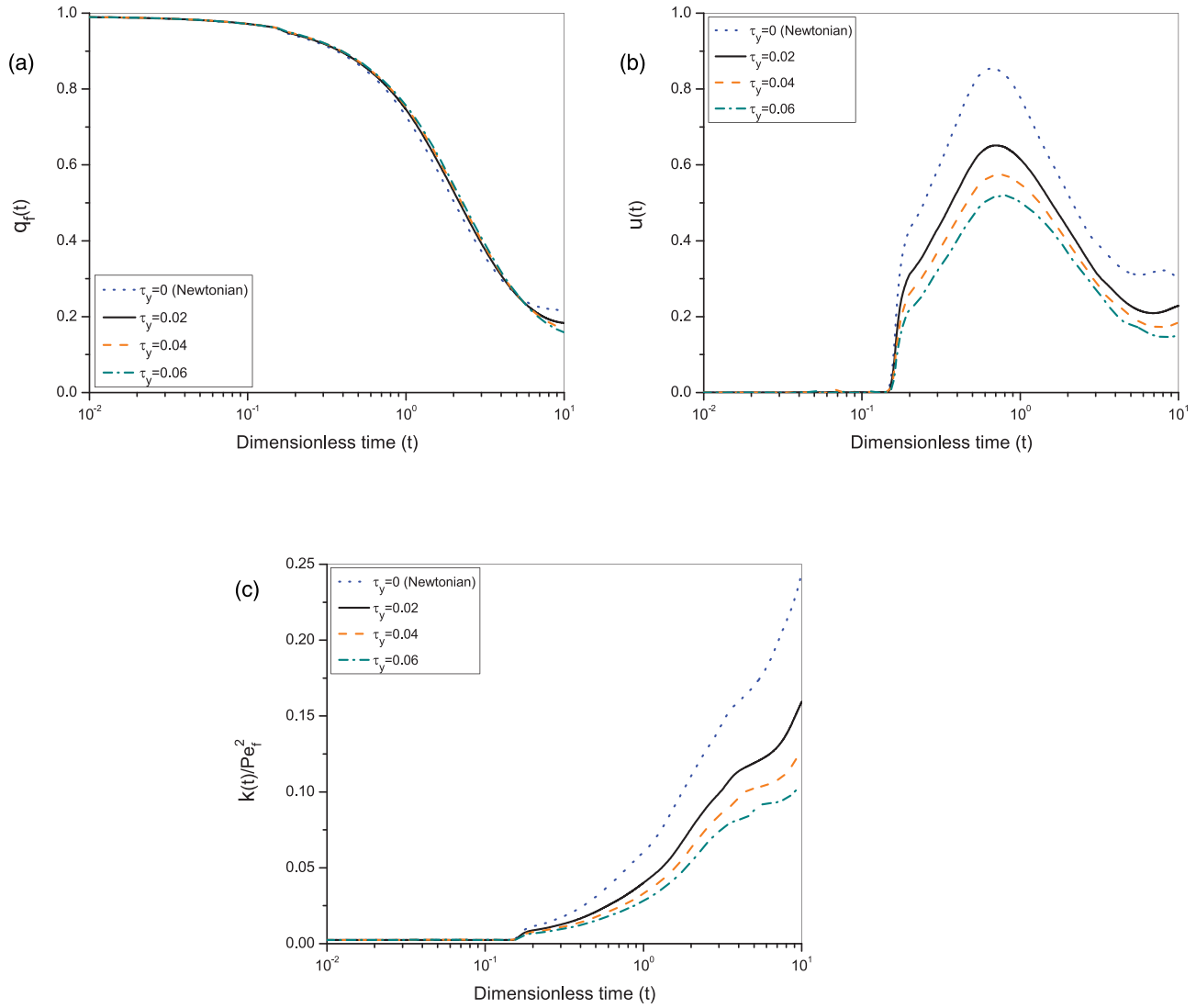


**FIG. 9.** Temporal variation of transport coefficients for different values of the yield stress ($\tau_y$) (48% severity of the stenosis, $Re = 50$, $Pe_f = 20$, and $\kappa = 0.1$). (a) The fraction of solute remaining in the fluid phase. (b) The apparent convection velocity based on averages over both the phases. (c) The dispersion coefficient based on averages over both phases.

in the system, the absorption raises at the interface of the lumen and tissue, and the solute is absorbed rapidly at the tube wall. Owing to this, for large values of $\kappa$, more amount of solute diffuses to the tube wall and very less amount of solute remains in the fluid phase. This leads to a decrease in $q_f(t)$. The large absorption parameter ($\kappa = 10$) helps the solute to leave the luminal side more rapidly (as it is directly proportional to the interfacial flux from lumen) and leaves behind only 10% solute at $t = 0.35$ in the lumen.

The effect of the wall absorption parameter ($\kappa$) on the solute convection is discussed and its significant effect is observed in this investigation. The apparent convection velocity ($u(t)$) based on averages over both phases depends on the velocity of the fluid and the initial distribution of the solute. It takes a minimum value till $t \sim 0.2$, thereafter, increases with time, attains a peak value, and finally decreases to approach a finite limit. It is interesting to note that for steady Poiseuille flow without any constriction, our results do agree with those of Phillips *et al.*,[1] while for unsteady cases, these values are constant until $t \sim 0.2$, and thereafter, it increases. Also for small values of $\kappa$, the convection process becomes stable at very large time, whereas for large values of $\kappa$, less time is required to reach the stable state. This is similar like for the case of $q_f(t)$ with different values of $\kappa$. The physical explanation is that until $t \sim 0.2$, the injected solute is dispersed downstream by molecular diffusion only and when the inlet velocity touches the solute cloud, which enables the cloud to transport under the action of convection as well as diffusion. So, until $t \sim 0.2$, the solute is not convected by the fluid velocity. Thereafter, as time increases, the solute is convected with the velocity of the fluid and it leads to an increase in $u(t)$. At large time, the convection process of the solute is stabilized, that means the solute is started to convect with the constant velocity of the fluid. For small values of $\kappa$, an equilibrium state between convection process and absorption at the wall occurs at very large time, whereas this equilibrium state occurs quickly for large values of $\kappa$. In addition, as $\kappa$ increases from 0.01 to 10, $u(t)$ decreases. For smaller values of $\kappa$, there remains a barely minimum, which disappears for larger values of $\kappa$ [cf. Fig. 6(b)].

The dispersion coefficient [$k(t)$] arises from the distribution of the solute cloud between parts of the system moving with different velocities. It depends on both fluid velocity and molecular diffusion of the solute. Figure 6(c) exhibits the results for the dispersion coefficient based on averages over both phases due to unsteady flow of Casson fluid past a stenosed artery as a logarithmic plot. It is worth noting that initially, until $t \sim 0.2$, the solute dispersion process is controlled by molecular diffusion of the solute and as time increases, the transportation process is more controlled by convection of the fluid as well as diffusion [which leads to an increase in $k(t)$], and again at large time, diffusive transport is effective in the system [which leads to a decrease in $k(t)$]. This phenomenon on solute dispersion is seen in our study and it is more significant for large values of $\kappa$. It is also noticed that for small values of $\kappa$, an equilibrium state between dispersion process and absorption at the wall occurs at large time, whereas for large values of $\kappa$, an equilibrium state is not reached and a continuous decrement is observed in the dispersion coefficient. This is due to the rapid transportation of solute from fluid phase to wall phase at large values of $\kappa$. It is also observed that as $\kappa$ increases, the dispersion coefficient decreases at large time. When $\kappa$ is small ($\kappa = 0.01$), there is slowness of solute transported to the stationary wall, whereas for higher $\kappa(= 10)$, a reverse phenomenon is observed. The fact that the wall absorption consumes solute in the near-wall fluid where the fluid velocity is small but the velocity gradient is high. In the presence of stenosis, the center of mass of the solute cloud moves faster to the central fluid of the stenosed tube, thereby leading to an increase in the advection speed, which eventually decreases the dispersion coefficient for larger $\kappa$. This is the physical reason for the decrement of $k(t)$.

Figure 7 represents the streamwise change in axial mean concentration $\left(C_m(t,z) = \frac{\int_0^{R_i(z)} rC_f(t,z,r)dr}{\int_0^{R_i(z)} rdr}\right)$ in fluid phase for a range of the absorption parameter $\kappa$ at time $t = 5$ for an unsteady flow of Casson fluid flowing through a stenosed artery. It is interesting to note that the peak value of $C_m$ decreases with increasing $\kappa$. The physical justification is that for large values of $\kappa$, the rate of absorption at the tube wall enhances in the system. Owing to this, more amount of solute leaves the lumen and it is depleted rapidly at the tube wall. As a result, there is decrement of the mean concentration. Moreover, when $\kappa = 10$, most of the solute absorbed in the downstream vicinity of the injected site and less spreading of solute takes place, which makes the peak flattened. Visual representation of the temporal spreading of the solute cloud is presented in Fig. 8, which further establishes our findings. As time progresses from $t = 1$ to $t = 10$, the initially injected uniform solute cloud at the throat of the stenosis ($z = 0$) does spread downstream non-uniformly under the action of both molecular diffusion and fluid convection along with the absorption at the stationary wall.

## B. Effect of yield stress

The time-dependent transport coefficients of solute for a range of values of the non-Newtonian parameter ($\tau_y$) are presented in Fig. 9 for $\kappa = 0.1$ at $t = 5$. Here $\tau_y$ is considered as 0 to 0.06. $\tau_y = 0$ represents the Newtonian characteristic of the fluid and rest of the values of $\tau_y$ indicate the non-Newtonian characteristic of the fluid. Figure 9(a) shows the effect of $\tau_y$ on the fraction of solute remaining in the fluid

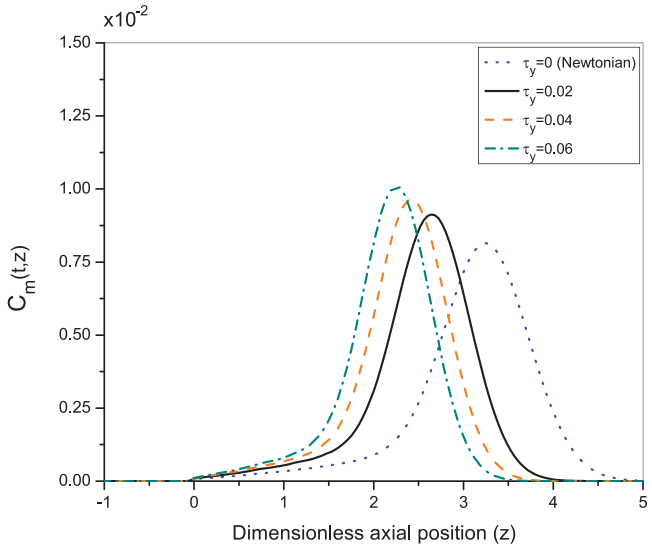


**FIG. 10.** The variation of axial mean concentration in fluid phase for different values of the yield stress ($\tau_y$) at $t = 5$ (48% severity of the stenosis, $Re = 50$, $Pe_f = 20$, and $\kappa = 0.1$).

phase $[q_f(t)]$. It is observed that there is no significant effect of $\tau_y$ on $q_f(t)$. The physical reason is that since the nonzero solute flux at the tube wall is independent of the non-Newtonian nature of the fluid, there is no significant effect of $\tau_y$ on $q_f(t)$. However, the non-Newtonian characteristic of the fluid has significant effect on the apparent convection velocity and the dispersion coefficient, and it has been displayed in Figs. 9(b) and 9(c). As $\tau_y$ increases, there is no change in values of the convection and dispersion coefficients until $t \sim 0.2$, and thereafter, the values diminish with increasing $\tau_y$, indicating that the dispersion phenomena are greatly modulated by the non-Newtonian rheology of the flowing fluid. The increase in yield stress of the fluid decreases the fluid movement and as a result, the solute is convected with lower velocity of the fluid. That is the reason for decrement in $u(t)$. Also, solute is dispersed with this lower velocity of the fluid and owing to this phenomenon, $k(t)$ decreases with increasing $\tau_y$. The peak value of the axial mean concentration in the fluid phase increases with increasing yield stress (cf. Fig. 10) and the peak does shift toward the downstream when the non-Newtonian effect gradually disappears. As yield stress of the fluid increases, flow velocity decreases and it decreases the solute dispersion. That is the physical significance for increment in axial mean concentration.

### C. Effect of severity of stenosis $\xi$

The axial dispersion of solute is directly proportional to the severity of the stenosis ($\xi$), which contributes much to three transport coefficients. In this study, no stenosis (0%) and various severities of stenosis (36%, 48%, and 64%) at the tissue-lumen interface are considered. Figure 11 shows that with the increase in severity of stenosis, the value of the fraction of solute remaining in the fluid phase $[q_f(t)]$

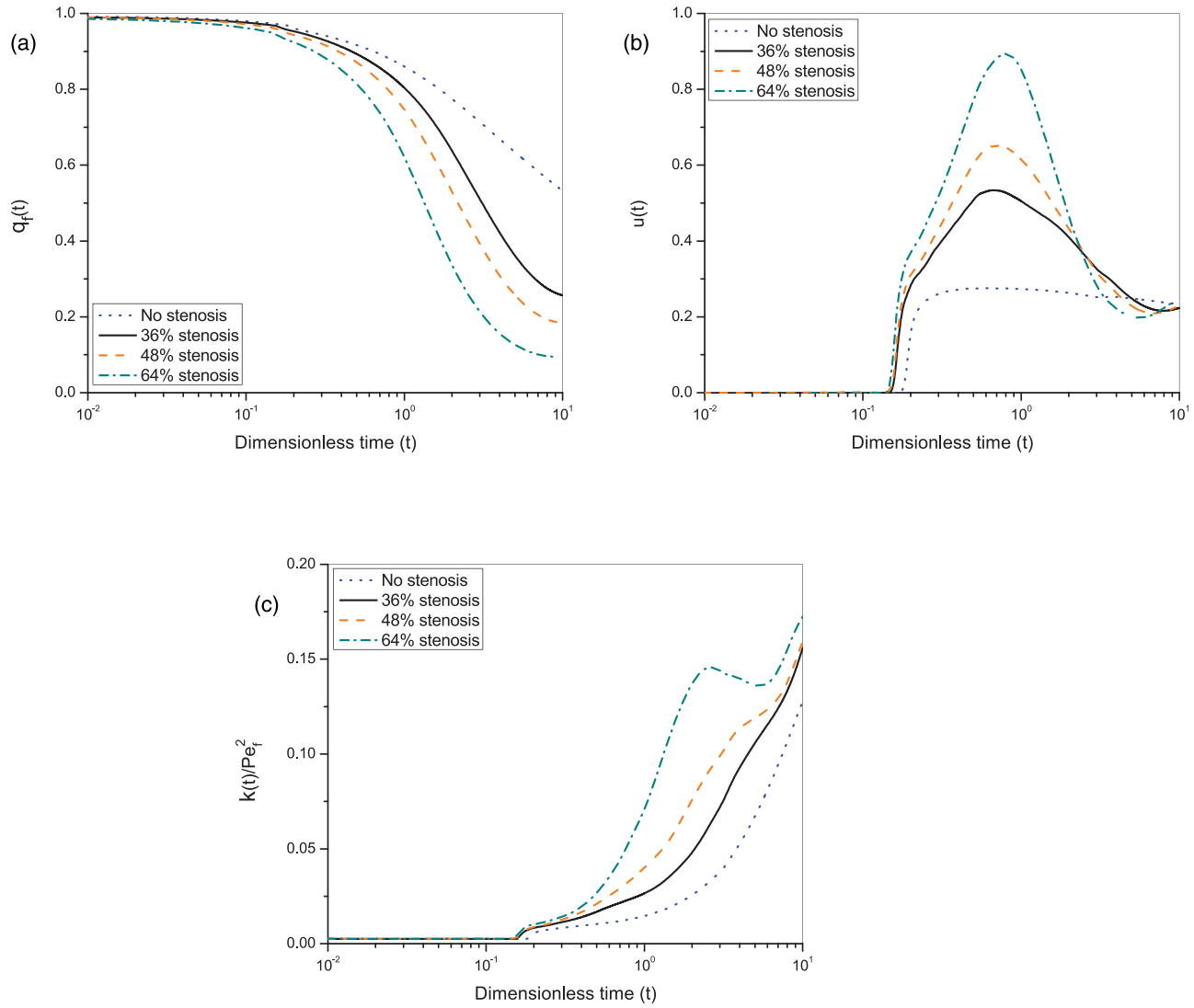


**FIG. 11.** Temporal variation of transport coefficients for various severities of the stenosis ($\kappa = 0.1$, $Re = 50$, $Pe_f = 20$, and $\tau_y = 0.02$). (a) The fraction of solute remaining in the fluid phase. (b) The apparent convection velocity based on averages over both phases. (c) The dispersion coefficient based on averages over both phases.

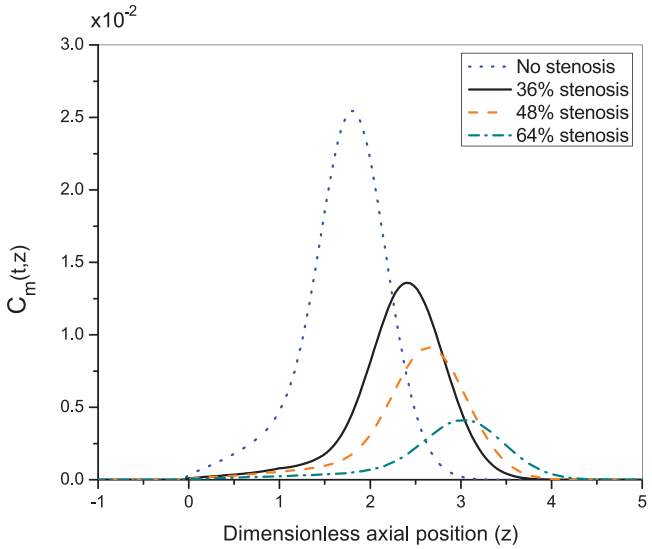


**FIG. 12.** The variation of axial mean concentration in fluid phase for various severities of the stenosis at $t = 5$ ($\kappa = 0.1$, $Re = 50$, $Pe_f = 20$, and $\tau_y = 0.02$).

decreases significantly. It is noticed that the inlet profile touches the solute cloud at $t = 0.17$, and before that time, only diffusive transport of the solute is present in the system to conduct the absorption. Because of this fact, more severe stenosis helps conduct more absorption due to the increased interfacial area. The values of the apparent convection velocity based on averages over both phases ($u(t)$) and the dispersion coefficient ($k(t)$) increase at early times, and thereafter diminish and get a finite limit. The above observation may be justified in the sense that as the severity of the stenosis increases, the flow is accelerated at the site of the stenosis and although the velocity in the vicinity of the interface is near zero, the solute gradient is high, which eventually increases $u(t)$ and $k(t)$; however, for larger times when a lesser amount of solute remaining in the fluid phase, the above coefficients diminish. There is a high rate of absorption in the case of severe stenosis (64% stenosis), and subsequently, it is observed that a smooth peak occurs in $k(t)$ due to the rapid change in concentration in the fluid phase. This phenomenon gradually decreases as it is moved to the moderate (48% stenosis) and mild stenosis (36% stenosis) model. In a bid to confirm our findings, the effect of severity of stenosis on axial mean concentration is presented in Fig. 12, indicating that the peak value of the mean concentration over cross section in the fluid phase diminishes with the increase in the value of the severity of the stenosis and the peak is shifted downstream, as anticipated. The physical explanation is that as $\xi$ increases, the solute convection and dispersion increase in the system, which leads to a decrease in axial mean concentration.

## V. CONCLUSION

The solute transportation process in the presence of non-Newtonian characteristic of the blood in small stenosed vessels and its surrounding tissue regions is analyzed by considering the two-dimensional Casson fluid flow and a two-phase stenotic system. The governing equations are numerically solved in staggered grid formulation with the help of the Marker and Cell (MAC) method and the immersed boundary method (IBM). In the case of a steady Poiseuille flow, the obtained results for transport coefficients, viz., the apparent convection velocity and the dispersion coefficient, agree well with those of Phillips *et al.*[1] This shows the accuracy of our analysis.

In this study, the fraction of solute remaining in the fluid phase [$q_f(t)$], the apparent convection velocity coefficient [$u(t)$], the dispersion coefficient [$k(t)$], and the axial mean concentration of the solute ($C_m$) are determined. The following salient observation may be noted from the present investigation:

(i) The fraction of solute remaining in the fluid phase [$q_f(t)$] diminishes with the increase of the wall absorption parameter $\kappa$.
(ii) The apparent convection velocity coefficient [$u(t)$] of the solute approaches a finite limit for all values of $\kappa$ and an early quasi-steady state is observed for larger $\kappa(= 10)$.
(iii) The value of the dispersion coefficient [$k(t)$] decreases for larger $\kappa(= 10)$ due to an increase in the advection speed.
(iv) The peak value of the axial mean concentration in fluid phase ($C_m$) decreases with increasing $\kappa$ as the higher the value of $\kappa$, more amount of solute leaves the lumen.
(v) The peak value of the axial mean concentration in fluid phase ($C_m$) increases with increasing yield stress ($\tau_y$) and the peak does shift toward the downstream when the non-Newtonian effect gradually disappears.
(vi) There is a high rate of dispersion of solute for more severe stenosis due to increased interfacial area.
(vii) With increasing severity of the stenosis, the peak value of the axial mean concentration in the fluid phase ($C_m$) diminishes and the peak is shifted downstream.

## ACKNOWLEDGMENTS

Prosanjit Das (SRF) gratefully acknowledges the research fellowship received from CSIR, New Delhi, India [Grant No. 09/202(0083)/2018-EMR-I].

## APPENDIX: DERIVATION OF MOMENTUM AND CONTINUITY EQUATIONS

The differential form of the law of conservation of momentum, considering that there is no external force acting on the fluid, is (cf. Bird *et al.*[66])

$$\frac{\partial(\rho \mathbf{v})}{\partial t} = -[\nabla \cdot \Phi], \tag{A1}$$

where $(\rho \mathbf{v})$ is the momentum per unit volume at a point in the fluid and $\Phi$ is the combined momentum flux tensor.

Combined momentum flux tensor ($\Phi$) is the sum of the molecular momentum flux tensor $(p\delta + \tau)$ and the convective momentum flux tensor $(\rho \mathbf{vv})$. Then Eq. (A1) becomes

$$\frac{\partial(\rho \mathbf{v})}{\partial t} = -[\nabla \cdot \rho \mathbf{vv}] - \nabla p - [\nabla \cdot \tau], \tag{A2}$$

where $\nabla p$ is the pressure gradient and $[\nabla \cdot \tau]$ represents the divergence of the stress tensor. Equations (2) and (3) can be obtained from Eq. (A2) by expressing the vector form into cylindrical polar coordinates system $(r, \theta, z)$.

From the equation of continuity, we know that the rate of increase in mass per unit volume is equal to the net rate of mass increase per unit volume by convection and can be written mathematically as

$$\frac{\partial \rho}{\partial t} = -(\nabla \cdot \rho \mathbf{v}). \tag{A3}$$

In the present analysis, we consider that the density of the fluid ($\rho$) is constant and Eq. (A3) becomes

$$\nabla \cdot \mathbf{v} = 0, \tag{A4}$$

and by expressing this equation into cylindrical polar coordinates system, we obtain Eq. (4) as

$$r\frac{\partial u_z}{\partial z} + \frac{\partial (r u_r)}{\partial r} = 0,$$

where $u_z$ and $u_r$ are the axial and radial components of the velocity vector $\mathbf{v}$, respectively.

## DATA AVAILABILITY

The data that support the findings of this study are available from the corresponding author upon reasonable request.

## REFERENCES


[1]C. Phillips, S. Kaye, and C. Robinson, "Time-dependent transport by convection and diffusion with exchange between two phases," J. Fluid Mech. **297**, 373–401 (1995).
[2]D. Or and T. A. Ghezzehei, "Traveling liquid bridges in unsaturated fractured porous media," Transp. Porous Media **68**, 129–151 (2007).
[3]B. B. S. Singhal and R. P. Gupta, *Applied Hydrogeology of Fractured Rocks* (Springer Science & Business Media, 2010).
[4]M. Dejam and H. Hassanzadeh, "Formation of liquid bridges between porous matrix blocks," AIChE J. **57**, 286–298 (2011).
[5]A. D. Gat, H. K. Navaz, and M. Gharib, "Wicking of a liquid bridge connected to a moving porous surface," J. Fluid Mech. **703**, 315–325 (2012).
[6]P. Das, M. Sarifuddin, and P. Kumar, "Solute dispersion in Casson fluid flow through a stenosed artery with absorptive wall," Z. Angew. Math. Phys. **71**, 100 (2020).
[7]R. Ross, "Rous–Whipple award lecture. Atherosclerosis: A defense mechanism gone awry," Am. J. Pathol. **143**, 987 (1993).
[8]G. I. Taylor, "Dispersion of soluble matter in solvent flowing slowly through a tube," Proc. R. Soc. London., Ser. A **219**, 186–203 (1953).
[9]R. Aris, "On the dispersion of a solute in a fluid flowing through a tube," Proc. R. Soc. London, Ser. A **235**, 67–77 (1956).
[10]R. Aris, "On the dispersion of a solute in pulsating flow through a tube," Proc. R. Soc. London, Ser. A **259**, 370–376 (1960).
[11]V. Ananthakrishnan, W. Gill, and A. J. Barduhn, "Laminar dispersion in capillaries: Part I. Mathematical analysis," AIChE J. **11**, 1063–1072 (1965).
[12]W. Gill and R. Sankarasubramanian, "Exact analysis of unsteady convective diffusion," Proc. R. Soc. London, Ser. A **316**, 341–350 (1970).
[13]R. Sankarasubramanian and W. N. Gill, "Unsteady convective diffusion with interphase mass transfer," Proc. R. Soc. London, Ser. A **333**, 115–132 (1973).
[14]A. Mukherjee and B. Mazumder, "Dispersion of contaminant in oscillatory flows," Acta Mech. **74**, 107–122 (1988).
[15]B. S. Mazumder and S. K. Das, "Effect of boundary reaction on solute dispersion in pulsatile flow through a tube," J. Fluid Mech. **239**, 523–549 (1992).
[16]A. Sarkar and G. Jayaraman, "The effect of wall absorption on dispersion in oscillatory flow in an annulus: Application to a catheterized artery," Acta Mech. **172**, 151–167 (2004).
[17]C.-O. Ng, "Dispersion in steady and oscillatory flows through a tube with reversible and irreversible wall reactions," Proc. R. Soc. London, Ser. A **462**, 481–515 (2006).
[18]C.-O. Ng and N. Rudraiah, "Convective diffusion in steady flow through a tube with a retentive and absorptive wall," Phys. Fluids **20**, 073604 (2008).
[19]B. Mazumder and S. Paul, "Dispersion of reactive species with reversible and irreversible wall reactions," Heat Mass Transfer **48**, 933–944 (2012).
[20]I. Griffiths, P. Howell, and R. Shipley, "Control and optimization of solute transport in a thin porous tube," Phys. Fluids **25**, 033101 (2013).
[21]M. Dejam, H. Hassanzadeh, and Z. Chen, "Shear dispersion in a capillary tube with a porous wall," J. Contam. Hydrol. **185–186**, 87–104 (2016).
[22]Z. Kou and M. Dejam, "Dispersion due to combined pressure-driven and electro-osmotic flows in a channel surrounded by a permeable porous medium," Phys. Fluids **31**, 056603 (2019).
[23]S. Charm and G. Kurland, "Viscometry of human blood for shear rates of 0–100 000 $s^{-1}$," Nature **206**, 617–618 (1965).
[24]G. W. S. Blair and D. C. Spanner, *Introduction to Biorheology* (Elsevier Scientific Publ. Co., 1974).
[25]D. A. McDonald, *Blood Flow in Arteries* (Williams & Wilkins, 1974).
[26]M. K. Sharp, "Shear-augmented dispersion in non-Newtonian fluids," Ann. Biomed. Eng. **21**, 407–415 (1993).
[27]R. Dash, K. Mehta, and G. Jayaraman, "Casson fluid flow in a pipe filled with a homogeneous porous medium," Int. J. Eng. Sci. **34**, 1145–1156 (1996).
[28]R. Dash, G. Jayaraman, and K. Mehta, "Shear augmented dispersion of a solute in a Casson fluid flowing in a conduit," Ann. Biomed. Eng. **28**, 373–385 (2000).
[29]P. Nagarani, G. Sarojamma, and G. Jayaraman, "Effect of boundary absorption in dispersion in Casson fluid flow in a tube," Ann. Biomed. Eng. **32**, 706–719 (2004).
[30]P. Nagarani, G. Sarojamma, and G. Jayaraman, "Exact analysis of unsteady convective diffusion in Casson fluid flow in an annulus–Application to catheterized artery," Acta Mech. **187**, 189–202 (2006).
[31]S. Shaw, S. Ganguly, P. Sibanda, and S. Chakraborty, "Dispersion characteristics of blood during nanoparticle assisted drug delivery process through a permeable microvessel," Microvasc. Res. **92**, 25–33 (2014).
[32]J. Rana and P. Murthy, "Solute dispersion in pulsatile Casson fluid flow in a tube with wall absorption," J. Fluid Mech. **793**, 877–914 (2016).
[33]J. Rana and P. Murthy, "Unsteady solute dispersion in small blood vessels using a two-phase Casson model," Proc. R. Soc. London, Ser. A **473**, 20170427 (2017).
[34]S. Debnath, A. K. Saha, B. Mazumder, and A. K. Roy, "Dispersion phenomena of reactive solute in a pulsatile flow of three-layer liquids," Phys. Fluids **29**, 097107 (2017).
[35]S. Debnath, A. Saha, B. Mazumder, and A. Roy, "On transport of reactive solute in a pulsatile Casson fluid flow through an annulus," Int. J. Comput. Math. **97**, 2303–2319 (2020).
[36]S. Debnath, A. K. Saha, B. Mazumder, and A. K. Roy, "Transport of a reactive solute in a pulsatile non-Newtonian liquid flowing through an annular pipe," J. Eng. Math. **116**, 1–22 (2019).
[37]S. Debnath, A. Saha, B. Mazumder, and A. Roy, "Dispersion of reactive species in Casson fluid flow," Indian J. Pure Appl. Math. **51**, 1451–1469 (2020).
[38]A. K. Roy, A. K. Saha, and S. Debnath, "Hydrodynamic dispersion of solute under homogeneous and heterogeneous reactions," Int. J. Heat Technol. **37**, 387–397 (2019).
[39]A. K. Roy, A. K. Saha, R. Ponalagusamy, and S. Debnath, "Mathematical model on magneto-hydrodynamic dispersion in a porous medium under the influence of bulk chemical reaction," Korea-Australia Rheol. J. **32**, 287–299 (2020).
[40]A. K. Roy and S. Shaw, "Shear augmented microvascular solute transport with a two-phase model: Application in nanoparticle assisted drug delivery," Phys. Fluids **33**, 031904 (2021).
[41]Z. Abbas, M. A. Jafar, and J. Hasnain, "Analysis of asymptotic solutions for non-Newtonian fluid flow between two parallel discs with dissimilar in-plane motion," Eur. J. Mech.-B/Fluids **84**, 129–138 (2020).
[42]Z. Abbas, M. Rafiq, J. Hasnain, and T. Javed, "Peristaltic transport of a Casson fluid in a non-uniform inclined tube with Rosseland approximation and wall properties," Arabian J. Sci. Eng. **46**, 1997–2007 (2021).
[43]S. Rafiq, Z. Abbas, M. Sheikh, and J. Hasnain, "Effects of variable viscosity on asymmetric flow of non-Newtonian fluid driven through an expanding/contracting channel containing porous walls," Arabian J. Sci. Eng. **45**, 9471–9480 (2020).

[44]J. Rana and P. Murthy, "Unsteady solute dispersion in Herschel–Bulkley fluid in a tube with wall absorption," Phys. Fluids **28**, 111903 (2016).
[45]J. Rana and P. Murthy, "Unsteady solute dispersion in non-Newtonian fluid flow in a tube with wall absorption," Proc. R. Soc. London, Ser. A **472**, 20160294 (2016).
[46]J. Rana and S. Liao, "A general analytical approach to study solute dispersion in non-Newtonian fluid flow," Eur. J. Mech.-B/Fluids **77**, 183–200 (2019).
[47]Sarifuddin, S. Chakravarty, P. K. Mandal, and H. I. Andersson, "Mass transfer to blood flowing through arterial stenosis," Z. Angew. Math. Phys. **60**, 299–323 (2009).
[48]Sarifuddin, "CFD modelling of Casson fluid flow and mass transport through atherosclerotic vessels," Differ. Equ. Dyn. Syst. (2020).
[49]J. R. Reddy, D. Srikanth, and S. K. Das, "Modelling and simulation of temperature and concentration dispersion in a couple stress nanofluid flow through stenotic tapered arteries," Eur. Phys. J. Plus **132**, 365 (2017).
[50]A. Tiwari, P. D. Shah, and S. S. Chauhan, "Solute dispersion in two-fluid flowing through tubes with a porous layer near the absorbing wall: Model for dispersion phenomenon in microvessels," Int. J. Multiphase Flow **131**, 103380 (2020).
[51]P. D. Shah, A. Tiwari, and S. S. Chauhan, "Solute dispersion in micropolar-Newtonian fluid flowing through porous layered tubes with absorbing walls," Int. Commun. Heat Mass Transfer **119**, 104724 (2020).
[52]C. S. Peskin, "Flow patterns around heart valves: A numerical method," J. Comput. Phys. **10**, 252–271 (1972).
[53]H. I. Andersson, R. Halden, and T. Glomsaker, "Effects of surface irregularities on flow resistance in differently shaped arterial stenoses," J. Biomech. **33**, 1257–1262 (2000).
[54]A. Yakhot, L. Grinberg, and N. Nikitin, "Modeling rough stenoses by an immersed-boundary method," J. Biomech. **38**, 1115–1127 (2005).
[55]Y. C. Fung and R. Skalak, "Biomechanics: Mechanical Properties of Living Tissues," J. Appl. Mech. **49**, 464–465 (1982).
[56]M. Davidson and R. Schroter, "A theoretical model of absorption of gases by the bronchial wall," J. Fluid Mech. **129**, 313–335 (1983).
[57]M. Kumar, S. Roy, and M. S. Ali, "An efficient immersed boundary algorithm for simulation of flows in curved and moving geometries," Comput. Fluids **129**, 159–178 (2016).
[58]A. Gilmanov and F. Sotiropoulos, "A hybrid cartesian/immersed boundary method for simulating flows with 3D, geometrically complex, moving bodies," J. Comput. Phys. **207**, 457–492 (2005).
[59]J. Welch, F. Harlow, J. Shannon, and B. Daly, "The mac method," Report No. LA-3425, Los Alamos Scientific Lab, Los Alamos, New Mexico, 1966.
[60]C. W. Hirt, "Heuristic stability theory for finite-difference equations," J. Comput. Phys. **2**, 339–355 (1968).
[61]G. Markham and M. Proctor, "Modifications to the two-dimensional incompressible fluid flow code ZUNI to provide enhanced performance," CEGB Report No. TPRD/L/0063/M82, 1983.
[62]J. C. Strikwerda, *Finite Difference Schemes and Partial Differential Equations* (SIAM, 2004), Vol. 88.
[63]Sarifuddin and P. K. Mandal, "Effect of interstitial fluid flow on drug-coated balloon delivery in a patient-specific arterial vessel with heterogeneous tissue composition: A simulation study," Cardiovasc. Eng. Technol. **9**, 251–267 (2018).
[64]Sarifuddin, S. Chakravarty, and P. K. Mandal, "Numerical simulation of Casson fluid flow through differently shaped arterial stenoses," Z. Angew. Math. Phys. **65**, 767–782 (2014).
[65]V. Srivastava and M. Saxena, "Two-layered model of Casson fluid flow through stenotic blood vessels: Applications to the cardiovascular system," J. Biomech. **27**, 921–928 (1994).
[66]R. B. Bird, W. E. Stewart, and E. N. Lightfoot, *Transport Phenomena* (John Wiley & Sons, 2006), Vol. 1.